CONTRIBUTION OF X-BAND INTERFEROMETRY FOR GEODYNAMICS AND ENGINEERING STUDIES

Mahdi Motagh [1,3], Eric J. Fielding [2], Mahmud Haghshenas-Haghighi [3], Roqayeh Shamshiri [3]

[1] Department of Geodesy and Remote Sensing, Helmholtz Center Potsdam, GFZ, Potsdam, Germany, Email: motagh@gfz-potsdam.de

[2] Jet Propulsion Laboratory, California Institute of Technology, Pasadena, California, USA, Email: eric.j.fielding@jpl.nasa.gov

[3] Department of Surveying and Geomatics Engineering, University of Tehran, Tehran, Iran, Email: m.haghshenas@ut.ac.ir, r.shamshiri@ut.ac.ir

ABSTRACT

Space-borne Interferometric Synthetic Aperture Radar (InSAR) is nowadays one of the most preferred geodetic methods to assess ground deformation associated with natural and anthropogenic hazards. Our capabilities for hazard monitoring have been further enhanced thanks to the high-resolution X-band radar data provided by the German TerraSAR-X satellite. Time-series InSAR using X-band data with short-revisit and regular schedule makes the long-term monitoring of small displacement with millimetric precision more feasible. In this study, we present an overview of some findings and results obtained in several projects where TSX InSAR observations contributed to investigate dynamic deformation associated with earthquake cycle and postseismic processes in New Zealand, land subsidence due to subsurface fluid flow extraction in Tehran, Iran, landslide creep in Kyrgyzstan and New Zealand, and differential movement of bridge approach embankments in northwest Iran.

1. Introduction

This paper focuses on an overview of the results obtained in several projects in which we used SAR imagery from Terrasar-X satellite to study deformation associated with geodynamic and engineering targets.

2. Postseismic deformation following the September 2010 Darfield, New Zealand, earthquake

The Darfield moment magnitude Mw 7.1 earthquake occurred at 2010 September 4, 04:35 local time in the South Island of New Zealand. Centered in the Canterbury plains, ~ 40 km west of Christchurch and 8 km south-east of Darfield, the mainshock initiated at about 10 km depth, propagated to the ground and extended for ~ 30 km across alluvial plains west of Christchurch. Significant surface rupture on the previously unrecognized Greendale Fault was reported for the earthquake, with predominantly horizontal strike-slip component of up to 5 m and vertical component of about 1 m [1].

Beavan et al. [2010, 2011, 2012] investigated co-seismic deformation models of the Darfield earth-quake by the combined analysis of GPS and InSAR data [2-4]. The results show that the mainshock sequence was very complex with most of the moment release occurring by right-lateral strike-slip motion on the Greendale Fault. The event also involved rupturing of several other fault segments including a blind NE-striking reverse fault near Charing Cross that initiated the rupture process, a left-lateral fault segment striking NNW from the epicenter, a blind reverse fault west of the Greendale Fault near Hororata, and another fault segment trending NE from the major left-stepping offset in the Greendale Fault (Fig. 1). The 2010 Darfield event was followed by two large aftershocks of magnitude Mw > 6 on Feb-ruary 22 and June 13, 2011, which occurred on pre-viously unrecognized faults less than 10 km from Christchurch city center [2-4].

Motagh et al. [2013] investigated postseismic defor-mation following the September 2010 Darfield earth-quake [5]. Fig. 2 shows continued ground deformation after the earthquake obtained from 4 pairs of X-band (TSX and CSK) and L-band (ALOS) interferograms. The most striking features of ground de-formation in these interferograms are: (1) deformation close to the epicenter, (2) localized deformation at the large step-

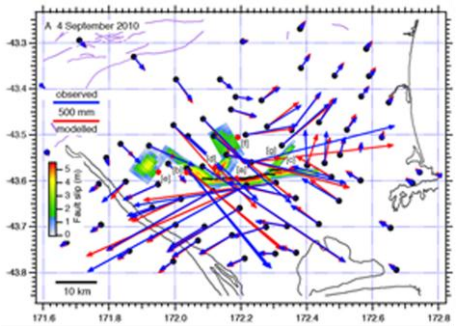

Figure 1. Observed (blue) and modelled (red) dis-placements at GPS sites, and the slip model derived from GPS and DInSAR data for the 4th September 2010 Darfield (Canterbury) earthquake [2]. [a] Greendale central, [b] Greendale NW-SE, [c] Greendale east, [d] Charing Cross fault, [e] Fault near Hororata, [ff] Fault NNW from epicenter, [g] Fault NE from step-over.

Proc. 'ESA Living Planet Symposium 2013', Edinburgh, UK
9–13 September 2013 (ESA SP-722, December 2013)

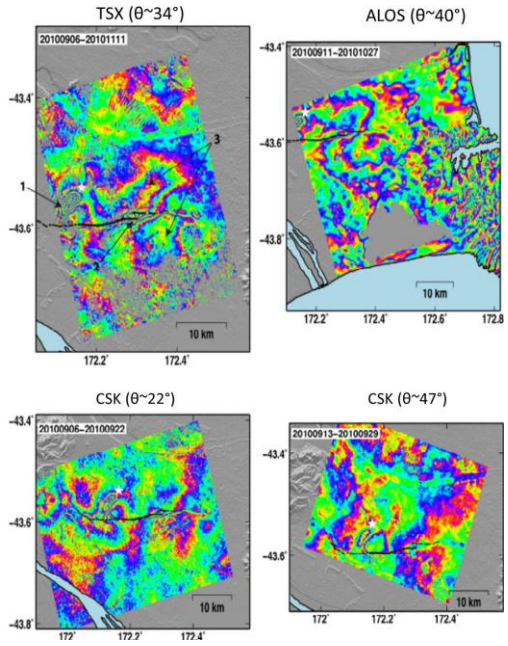

Figure 2. Postseismic ground deformation following the 2010 September Darfield earthquake. All interferograms have been unwrapped and rewrapped again with each color-cycle (fringe) representing ~ 1.5 cm of ground deformation in the line-of-sight (LOS) direction from the ground to the satellite. θ corresponds to the average incidence angle of each interferogram. Black arrows in the TSX result show 3 main features of postseismic deformation (see the manuscript). The black solid line shows surface trace of the Greendale fault [1]. The white star is the epicenter of the 2010 Darfield earthquake.

over of the Greendale fault and (3) two lobes of deformation on the Greendale fault.

3. Landslide in Kyrgyzstan

In this section, we present the results of our research in which we investigated the capability of X-band SAR Interferometry (InSAR) for landslide investigation in Southern Kyrgyzstan, Central Asia. Due to its specific tectonics and climate setting, Kyrgyzstan is among the most landslide-prone countries in the world. Up to now 3000 landslides, which area mainly concentrated in the Southern Tianshan along the Eastern rim of the Fergana Basin, have been recorded based on field investigation and analysis of aerial photographs [6].

Previous studies for the assessment of landslide hazard in Southern Kyrgyzstan relied mainly on the in-formation obtained by the analysis of optical remote sensing sensors [6]. In 2009, the German Federal Ministry of Research and Technology (BMBF) funded a project called PROGRESS (http://www.earth-in-progress.de/). One important scope of this project was to assess the potential of radar remote sensing methods for characterizing potentially hazardous surface processes in Central Asia. Within the framework of this project, Motagh et al. (2013) investigated the ca-pability of high-resolution (3 m) Synthetic Aperture Radar (SAR) imagery from German TerraSAR-X sat-ellite for recognition of surface movement in Kyrgyzstan [7]. The test site was located south of Uzgen City in southeast of Kyrgyzstan (Fig. 3).

The X-band interferograms showed a wide range of variation in the phase coherence: the interferometric coherence in the region proved to be generally good for short-term summer interferograms, but degraded quickly in the winter season even for images separat-ed by a single repeat cycle of TerraSAR-X satellite (11 days), presumably because of continuous snow cover.

Fig. 4 shows an example of 8 short-term descend-ing interferograms during May to September 2009. In this geometry, the interferograms are sensitive to mass movements occurring on slopes facing towards the west. White circles show the location of areas where phase variations appear to be associated with landslides. The results shown in Fig. 4 proved to be corroborated well with results from ground recon-naissance (Fig. 5). Indeed, field investigation per-formed following these observations revealed that all locations detected above correspond to landslide features in the region, previously unrecognised and un-mapped by geologists.

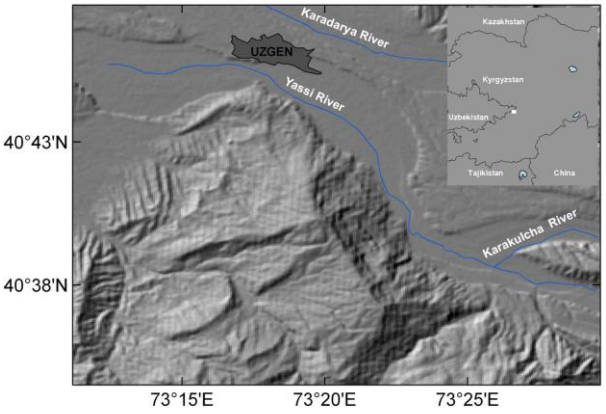

Figure 3. The geographical setting of the study area in southeastern Kyrgyzstan. The white square in the inset shows the location of Uzgen inside Kyrgyzstan.

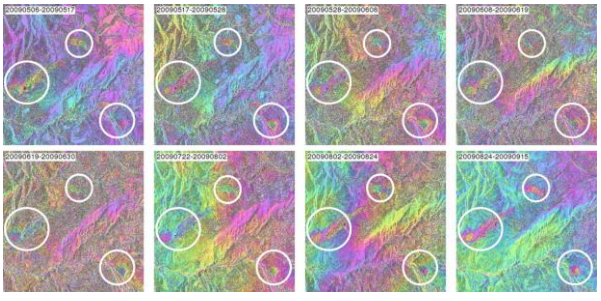

Figure 4. Eight examples of descending TSX interferograms. The signal related to landslide is marked by white circle. The interferograms are shown in the slant-range geometry format [7]

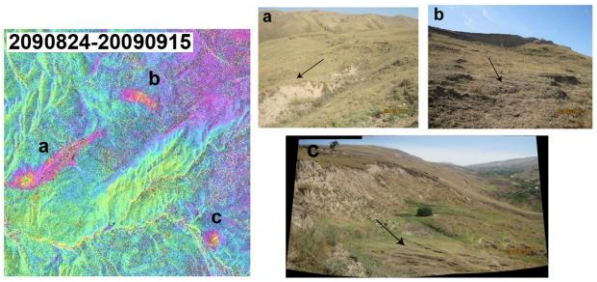

Figure 5. Ground pictures of 3 landslide features detected in descending TSX interferograms [7]

4. Taihape Landslide in New Zealand

In this section we present the results of a research project that we did in collaboration with the institute of GNS Science in New Zealand to assess the potential of X-band and C-band SAR images for monitoring Taihape landslide, North Island of New Zealand. Field survey measurements of displacement in this region indicated that Taihape landslide is slightly active. We used 31 TerraSAR-X SAR images between September 2010 and June 2011 and 31 Envisat SAR images between August 2003 and May 2010 to measure the deformation. Each dataset is processed using the time-series method of Small BAseline Subset (SBAS) to extract time-series of deformation.

The results of time-series analysis of both X-band and C-band datasets, illustrated in Fig. 6, confirm that the slope is slightly creeping with a range of a few millimetres per year. However, because of longer time span, Envisat time-series results indicate the descending trend of displacement on the slope better than TerraSAR-X. Comparison between results indicate that SBAS processing provides more coherent pixels in TSX data than Envisat data; 60000 coherent pixels in TSX result as compared to about 2600 coherent pixels in Envisat result.

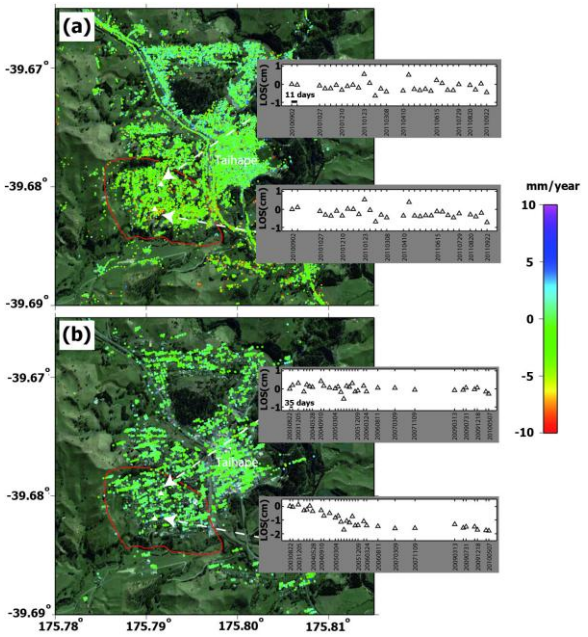

Figure 6. InSAR displacement rate maps and time-series of two example points of (a) TerraSAR-X and (b) Envisat results over Taihape landslide. Creeping area is indicated by red line.

5. Land subsidence in Tehran

Underground water exploitation in Tehran plain has led to land subsidence in agricultural areas west of Tehran City [8]. Here we present the result of InSAR time-series processing [9] applied on a large dataset of X-band, C-band and L-band SAR data covering a long period of time between 2003 and 2013. The SAR data used in this research are shown in Tab. 1.

Table 1. SAR data used in this study

Dataset	Number of images	Time span	Incidence angle
Env-Des	15	Jul 2003-May 2005	~21°
Env-Des	9	May 2004-Mar 2005	~23°
Env-Asc	15	Aug 2004-Aug 2007	~41°
ALOS	10	Jan 2008 –Mar 2010	~34°
TSX-VV	15	Jan 2012-Sep 2012	~26°

Average LOS velocity maps derived from different X-band, C-band and L-band datasets are shown in Fig. 7. The spatial extents of displacement derived from all datasets are almost the same. However, densities of pixels in TSX results are more than other datasets.

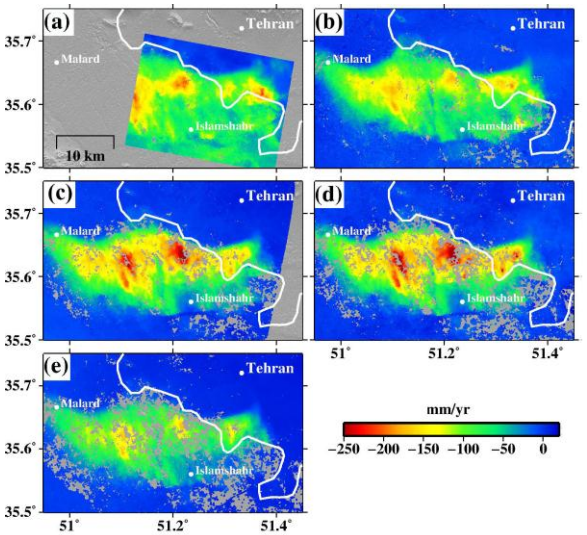

Figure 7. Average LOS velocity maps derived from different datasets for the subsidence bowl in the southwest of Tehran. (a) TerraSAR-X. (b) ALOS. (c) Envisat descending (d) Envisat descending (e) Envisat ascending. Red and blue colors indicate movement away and toward satellite, respectively. White line shows urban area of Tehran.

Although TerraSAR-X with the shortest wavelength is the most sensitive to vegetation coverage, time intervals between interferograms of this dataset are short enough to keep the high coherence.
Densities of Envisat results are less than other datasets because of temporal decorrelation due to long time intervals of interferograms. Because of different incidence angle, displacement rate of different datasets are slightly different. Envisat ascending and ALOS data are less sensitive to vertical displacement than other datasets. Therefore maximum LOS velocities obtained from their analysis (Fig. 7-b and e) have slightly lower values than other datasets.

6. TSX analysis of Lake Urmia Causway (LUC)

In this section the capability of the TSX data for de-formation analysis of an engineering target is presented. For this purpose, we analyzed a total of 18 TSX images acquired from 2012/05/20 to 2013/01/28, using the SBAS approach to assess the deflation of the Lake Urmia Causeway (LUC), northwest Iran. LUC consists of one bridge and two embankments on both sides of the bridge. Differential movement of the bridge approach embankment may seriously damage the bridge itself, so it is very important to accurately monitor the embankments. Fig. 8 illustrates the deformation map of the area with peak amplitude of ~ 85 mm/year in the LOS direction. The map shows a bowl-shaped pattern of deformation along the causeway with the maximum con-cavity occurred toward the bridge. For more details about this project please refer to Ref. [10].

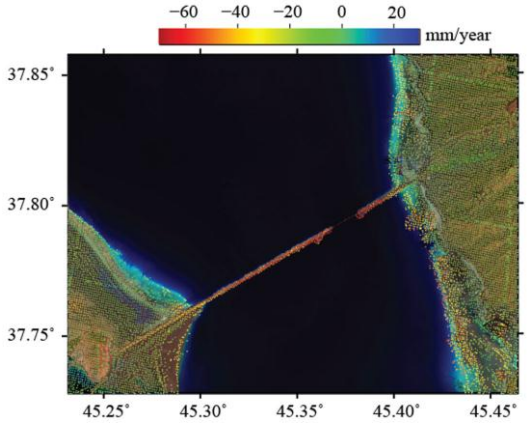

Figure 8. Mean LOS velocity obtained by the time-series analysis of TerraSAR-X data between 20.05.2012 and 28.01.2013.

7. Acknowledgment

TerraSAR-X data are the copyright of German Aerospace Agency (DLR) and were provided under the research proposals GEO0179, GEO1217 and GEO0714. We acknowledge the European Space Agency (ESA) for providing the Envisat data under the proposals AOALO3740 and C1P2892.

8. References

1. Quigley, M., Van Dissen, R., Litchfield, N., Villamor, P., Duffy, B., Barrell, D., Furlong, K., Stahl, T., Bilderback, E. & Noble, D. (2011). Surface rupture during the 2010 Mw 7.1 Darfield (Canterbury) earthquake: Implications for fault rupture dynamics and seismic-hazard analysis. *Geology*. **40**(1), 55–58.

2. Beavan, J., Wallace, L., Samsonov, S., Ellis, S., Motagh, M., & Palmer, N. (2010). The Darfield (Canterbury) earthquake: Geodetic observations and preliminary source model. *New Zeal Soc. Earthquake Eng.* **43**(4).

3. Beavan, J., Fielding, E., Motagh, M., Samsonov, S., & Donnelly, N. (2011). Fault Location and Slip Distribution of the 22 February 2011 Mw 6.2 Christchurch, New Zealand, Earthquake from Geodetic Data. *Seismol Res Lett.* **82**(6), 789-799.

4. Beavan, J., Motagh, M., Fielding, E. J., Donnelly, N., & Collett, D. (2012). Fault slip models of the 2010–2011 Canterbury, New Zealand, earthquakes from geodetic data and observations of postseismic ground deformation. *New Zeal J Geol Geop.* **55**(3), 207-221.

5. Motagh, M., Beavan, J., Fielding, E. J., & Haghshenas, M. (2013). Postseismic Ground Deformation Following the September 2010 Darfield, New Zealand, Earthquake From TerraSAR-X, COSMO-SkyMed, and ALOS InSAR. *IEEE Geosci Remote S.* **11**(1), 186-190.

6. Roessner, S., Wetzel, H. U., Kaufmann, H., & Sarnagoev, A. (2005). The Future for Asteroid Exploration. *Nat Hazards.* **35**(3), 395-416.

7. Motagh, M., Wetzel, H. U., Roessner, S., & Kaufmann, H. (2013). A TerraSAR-X InSAR study of landslides in southern Kyrgyzstan, Central Asia. *Remote Sensing Letters.* **4**(7), 657-666.

8. Motagh, M., Walter, T. R., Sharifi, M. A., Fielding, E., Schenk, A., Anderssohn, J., & Zschau, J. (2008). Land subsidence in Iran caused by widespread water reservoir overexploitation. *Geophys. Res. Lett.* **35**(16).

9. Hooper, A. (2008). A multi-temporal InSAR method in-corporating both persistent scatterer and small baseline approaches. *Geophys. Res. Lett.* **35**(16).

10. Shamshiri, R., Motagh, M., Baes, M., Sharifi, M. (2013). Bridge deformation monitoring: insight from InSAR time-series and Finite Element Modelling. In 'ESA living planet symposium', Edinburgh, United Kingdom.